Thermodynamic and Kinetic Considerations of the Formation and the Dissolution of Nanoparticles of Substances Having Low Solubility

Wolfram Vogelsberger*

Institute of Physical Chemistry, Chemistry and Earth Science Faculty, Friedrich-Schiller-University Jena, Lessingstrasse 10, D-07743 Jena, Germany

Received: March 19, 2003; In Final Form: May 27, 2003

The formation and dissolution of nanoparticles in solution is investigated. The solution consists of a particle-forming species, solute, and a solvent. The Gibbs free energy of the particle-containing system is calculated compared to a supersaturated initial solution. The whole amount of substance of the particle-forming species is dissolved in this reference state. The system particles solution is assumed to consist of particles of identical size. The particles have a determined concentration. The amount of particle-forming species is constant in the system. It is distributed on the particles and the dissolved part. The Gibbs free energy of all the systems that can build up by this way is calculated. A free energy surface in the particle size−particle concentration space is the result. It turns out that there are states of the system where the particles tend to dissolve and other states where the particles tend to grow further. Extrema of the free energy with respect to the particle size and to the particle concentration, respectively, can be determined. The free energy surface forms a valley. Changes in the system are assumed to occur in the negative gradient direction of the Gibbs free energy gradient curves. Examination of states with particles that are able to grow shows the gradient curves quickly to approach the bottom of the free energy surface. The bottom line ends at the stable equilibrium of the bulk solid phase under saturation conditions. By these considerations it is possible to determine the particle formation process. It consists of a nucleation phase and a phase of Ostwald ripening. On the other hand, it is possible to model the dissolution process of a given amount of particles. The results of this modeling are compared to the dissolution experiments of silica nanoparticles. Good agreement between experiment and theory is found.

1. Introduction

The application of different solids as nanodispersed powders is an eminent tool in materials science. The increased energy of these nanoparticles compared to the bulk phases is responsible for many size effects. Often these small particles are used in the form of colloidal dispersions in a liquid. Oxidic nanoparticles such as, for example, silica, alumina, or titania are used in amounts of thousands of tons per year in different fields of application such as drug design, catalysis, or paintings. The solubility of such nanoparticles in solvents such as water is low. Nevertheless, in some cases of application of colloidal dispersions it may be of some interest. This is especially the case since the solubility of small particles is considerably increased compared to the solubility of the bulk phases. If colloidal dispersions are used, the amount of substance also dissolved under saturation conditions is always small compared to the total amount of substance of the nanoparticles present in the dispersion. From this point of view the dispersion is highly supersaturated in relation to the substance that forms the nanoparticles.

It is the aim of this paper to make a proposal to model the colloidal dispersion thermodynamically. To this end the total amount of substance of the colloid in the dispersion is distributed in a special state of the system on the colloidal particles and the dissolved part. The colloidal particles are assumed to have spherical shape and uniform size in this state. The dissolved part is assumed to consist of uncharged monomer. If the amount of the colloid-forming species in the system is large then a very large number of such states can be built. It should be noted that one state of the system could be built up by two ways: first the nucleation and particle growth from a supersaturated initial solution, and on the other hand by dissolution of an appropriate amount of nanoparticles. This amount of nanoparticles must give the same initial supersaturation in the solution if they are completely dissolved. The thermodynamic potential function of each of the states characterized by a determined particle size, a determined particle concentration, and the remaining amount of substance dissolved is compared to the described initial supersaturated state, which is obtained if the total amount of the colloid-forming species in the system is presently dissolved. By this way, a surface of the potential function in dependence on particle size and particle concentration can be calculated.

States of the system having special properties such as stability or instability compared to neighboring states are looked for. The path of the system from one state to the neighboring state is thought to follow the steepest change of the thermodynamic potential. This is the path in the direction of the gradient of potential function. By this way the kinetic changes of the system can be modeled. The approach presented is a phenomenological one. It does not use molecular properties. Such a microscopic approach of the problem under consideration is of course of

* Prof. Dr. Wolfram Vogelsberger, Institut für Physikalische Chemie, Chemisch-Geowissenschaftliche Fakultät, Friedrich-Schiller-Universität Jena, Lessingstrasse 10, D-07743 Jena, Deutschland. Phone: +49 3641 948340, Fax: +49 3641 948302, e-mail: c9vowo@uni-jena.de

10.1021/jp030347z CCC: $25.00
Published on Web 08/14/2003

basic interest. For the vapor droplet transition there exists interesting work in a series of papers of H. Reiss and co-workers, see, e.g., refs 1−3. But it seems to be difficult to transfer these considerations to the precipitation and dissolution processes.

2. Thermodynamic Model

Considered is a system composed of two species, the colloid-forming species, 1, and the solvent, 2. The total amount of substance of the colloid-forming species is $n_L{}^0(1)$, and the total amount of substance of the solvent is $n_L{}^0(2)$. The upper index, 0, indicates the amount of substance in the system if the colloid-forming species is completely dissolved. This is our reference state. The Gibbs free energy of all states of the system is compared to this state. The upper index, 1, is used if nanoparticles are present. The lower indices, L and C, indicate the solution and the solid, colloidal phase, respectively. The total amount of substance of both species, n^0, is constant

$$n_L^0(1) + n_L^0(2) = n^0 \tag{1}$$

Both total amounts of substance itself are constant. The amount of the solvent does not change, and the amount of substance of the colloid-forming species is distributed on the nanoparticles and on the dissolved part

$$n_L^1(1) + n_C^1(1) = n_L^0(1) \tag{2}$$

Isothermal and isobaric conditions are maintained. The Gibbs free energy, g, is the natural thermodynamic potential in this case. It is given by

$$dg = -sdT + \upsilon dp + \sum_i \mu_i dn_i + \sigma do_C \tag{3}$$

where s is the entropy, T is the temperature, υ is the volume of the system, p is the pressure, μ_i is the chemical potential of the amount of substance, n_i, of component, i, σ is the interfacial energy (surface tension), and o_C is the surface area of the nanoparticles. The Gibbs free energy is a first-order homogeneous function of the extensive variables and it obeys the Euler theorem.[4]

The extensive variables are n_i and o_C. The Gibbs free energy of colloid formation, $\Delta_C g$, can be written as

$$\Delta_C g = g^1 - g^0 = n_L^1(1)\mu_L^1(1) + n_L^1(2)\mu_L^1(2) + n_C^1(1)\mu_C^1(1) + \sigma o_C - n_L^0(1)\mu_L^0(1) - n_L^0(2)\mu_L^0(2) \tag{4}$$

To evaluate this equation, appropriate expressions for the chemical potentials are necessary. Especially the selection of the standard state is important. The commonly used standard states in solutions are the state of the pure solvent for the solvent, use of Raoult's law, and the hypothetical state of the pure solute for the dissolved component, use of Henry's law.[5] These standard states can easily be circumvented if the state of the saturated solution, upper index s, is introduced. For each component, i (i = 1,2), we can write

$$\mu_L(i) = \mu_L^{\otimes}(i) + R_G T \ln a_x(i)$$

and

$$\mu_L^s(i) = \mu_L^{\otimes}(i) + R_G T \ln a_x^s(i) \tag{5}$$

The symbol ⊗ indicates an arbitrary standard state and $a_x(i)$ is the mole fraction activity. R_G is the gas constant. Subtraction of the two equations results in

$$\mu_L(i) = \mu_L^s(i) + R_G T \ln \frac{a_x(i)}{a_x^s(i)} \tag{6}$$

It can be seen in eq 6 that the standard state is now the state of the saturated solution.

The following considerations are confined to very dilute solutions and the activity is therefore substituted by the mole fraction itself:

$$a_x^j(i) \approx x_L{}^j(i) = \frac{n_L{}^j(i)}{\sum_{i=2} n_L{}^j(i)}, \quad j = 0,1 \tag{7}$$

The upper index, j, stands for the states of the system, 0 or 1, and 1 has to be substituted by s in the saturated solution.

The chemical potentials of the two components in the initial and in the final states of the system may therefore be written as follows:

$$\mu_L^0(i) = \mu_L^s(i) + R_G T \ln \frac{x_L^0(i)}{x_L^s(i)}$$

$$\mu_L^1(i) = \mu_L^s(i) + R_G T \ln \frac{x_L^1(i)}{x_L^s(i)} \tag{8}$$

The chemical potential of the bulk solid, $\mu_C{}^1(1)$, is equal to the chemical potential of the solute under saturation conditions $\mu_C{}^1(1) = \mu_L{}^s(1)$. Using this equality and the chemical potentials given by eq 8, eq 4 may be written as

$$\Delta_C g = -k_B T \left\{ \sum_{i=1}^{2} N_L^0(i) \ln \frac{x_L^0(i)}{x_L^s(i)} - \sum_{i=1}^{2} N_L^1(i) \ln \frac{x_L^1(i)}{x_L^s(i)} \right\} + \sigma o_C$$

$$= R_G T (n_L^0(1) - n_C^1(1)) \ln \left[y \left(1 - \frac{n_C^1(1)}{n_L^0(1)} \right) \right] + \sigma o_C - R_G T n_L^0(1) \ln y + R_G T (n^0 - n_C^1(1)) \ln \left[\frac{(n_L^s(1) + n_L^0(2))}{n^0 - n_C^1(1)} \right] - R_G T n^0 \ln \left(\frac{n_L^s(1) + n_L^0(2)}{n^0} \right) \tag{9}$$

where k_B is the Boltzmann constant, $N_L{}^0(i)$ are the total numbers of molecules of species, i, in the system, $N_L{}^0(i) = n_L{}^0(i)N_A$. Here, N_A is the Avogadro constant, $n_L{}^s(1)$ is the amount of species 1 in the saturated solution, $y = n_L{}^0(1)/n_L{}^s(1)$ is the initial supersaturation. Now the following dimensionless quantities are introduced

$$\frac{\Delta_C g}{n_L^0(1) R_G T} = g(r,z)$$

$$\frac{n_C^1(1)}{n_L^0(1)} = \frac{4\pi N_A R^3}{3V_C(1)} \frac{Z}{N_L^0(1)} = zr^3$$

$$z = \frac{Z}{N_L^0(1)}$$

$$r = R\left(\frac{4\pi N_A}{3V_C(1)}\right)^{1/3} = \frac{R}{R_0}$$

$$h = \frac{4\pi\sigma}{k_B T}R_0^2$$

$$a = \frac{n_L^0(1)}{n^0}$$

$$b = \frac{n_L^s(1) + n_L^0(2)}{n^0} \qquad (10)$$

Here, $N_L{}^0(1)$ is the total number of molecules of species 1 in the system, and V_C is the molar volume of the particles. The number of clusters, Z, is related to $N_L{}^0(1)$, and the radius of the clusters is related to the radius of a molecule, R_0, if the molecule is taken to be a sphere. Using the quantities introduced in eq 10 we can write eq 9 in the form

$$g(r,z) = (1 - zr^3)\ln\{y(1 - zr^3)\} - \frac{1}{a}(1 - azr^3)\ln\{1 - azr^3\} + hzr^2 - zr^3 \ln b - \ln y \qquad (11)$$

Up to the term $-zr^3 \ln b$, eq 11 is similar to eq 8 given in ref 6. This similarity is due to the fact that in both systems there are two components. One component forms the colloidal particles and the other one is intended not to participate in the reaction. Therefore, its amount of substance remains constant. In both cases the saturated state is chosen as standard state and reduced quantities are used. The difference results from the approximation $y = n_g{}^0(1)/n_g{}^s(1) \approx p_g{}^0(1)/p_g{}^s(1)$, which has been applied in ref 6. Both expressions are identical if this approximation is not applied.

The Gibbs free energy surface, $g(r,z)$, according to eq 11, is shown in Figure 1 as a function of particle size, r, and particle concentration, z. Each point on this surface is characterized by a determined amount of substance contained in the particles, $n_C{}^1(1) = zr^3 n_L{}^0(1)$, and therefore by a special $r-z$ pair. The residual part of the total amount of the particle-forming species, $n_L{}^0(1)$, remains dissolved in the solution, $n_L{}^1(1)$, in accordance with eq 2. The calculations are made for silica at $T = 310.15$ K. The saturation concentration is taken to be $c_L{}^s(1) = 2$ m mol/L, and an interfacial energy of 50 m Nm^{-1} is used.[7] This later value of the interfacial energy is obtained from dissolution experiments of small particles at $T = 298.15$ K. The size of these particles is calculated from the specific surface area, and the validity of the Kelvin equation is assumed. The mean between the two given values 54 and 46 m Nm^{-1} determined for particles prepared at different temperatures is used. The density of the silica particles is taken to be 2.2 g cm^{-3}. A supersaturation of $y = 3$ has been assumed so that the main features of the $g(r,z)$ surface are visible, i.e., they are in the same order of magnitude. The surface shows a crest and a valley. As stated before, this surface gives the Gibbs free energy of all states of the systems composed of particles of different size and concentration that can be formed from the total amount of silica present in the system. The particles have the same size in one selected state. The actual supersaturation in all these states is different since the particle formation has consumed monomer, i.e., a depletion of the mother phase took place.

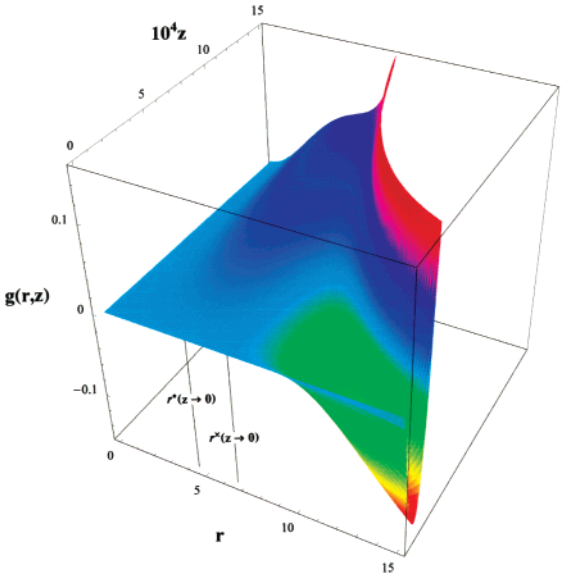

Figure 1. Gibbs free energy of nucleation of silica particles, $g(r,z)$, as a function of cluster size, r, and cluster concentration, z ($T = 310.15$ K, $y = 3$).

To investigate eq 11 in more detail, the partial derivatives of $g(r,z)$ with respect to the particle size and the particle concentration can be determined

$$\left(\frac{\partial g(r,z)}{\partial r}\right)_z = 0 = \frac{2h}{3r^*} - \ln\left\{\frac{yb(1 - zr^{*3})}{1 - azr^{*3}}\right\} \qquad (12a)$$

$$\left(\frac{\partial g(r,z)}{\partial z}\right)_r = 0 = \frac{h}{r^\times} - \ln\left\{\frac{yb(1 - zr^{\times 3})}{1 - azr^{\times 3}}\right\} \qquad (12b)$$

Equation 12 a is obtained by the derivation at constant particle concentration. It is the analogue to the well-known Kelvin equation. The expression $y(1 - zr^3) = n_L{}^1(1)/n_L{}^s(1)$ represents the actual supersaturation. Therefore, an additional factor $b/(1 - azr^3)$ appears in eq 12a. Under the conditions discussed here, it is $a = 1.0883 \times 10^{-4}$ and $b = 0.99993$.

The main features of the surface can be observed better by looking at the contour plot of this surface, Figure 2. The small black lines represent contour lines. The black numbers near the lines are the numerical values of $g(r,z)$. The maximum value of the product zr^3 is $zr^3 = 1$. The whole amount of substance of the colloid-forming species is contained in the nanoparticles, $n_C{}^1(1) = n_L{}^0(1)$. The graph $zr^3 = 1$ bounds the range of definition of eq 11 and therefore the surface $g(r,z)$. The initial state of a dissolution experiment is one point on this graph. The largest value of the factor $b/(1 - azr^3)$ is therefore $b/(1 - a) = 1.00004 \approx 1$.

The green graph labeled A represents eq 12a. As stated before, this equation is the analogue to the Kelvin equation. Since $b/(1 - azr^3) < b/(1 - a)$, the difference between the common Kelvin equation and eq 12a is negligible in the case discussed where the saturation concentration of the solid is very small. It becomes, however, remarkable with increasing solubility. Graph A starts at the radius $r^* = 2h/3 \ln(by) = 4.37$. This value of r^* belongs to the initial supersaturation of the system. The particle concentration approaches $z \rightarrow 0$. Up to the maximum of graph A, two extrema, a maximum and a minimum, can be found for one particle concentration. The Kelvin equation gives a critical and a metastable state at a constant number of particles. The word "metastable" applies to the fact that stability is only maintained at constant z. The existence of this relative stable

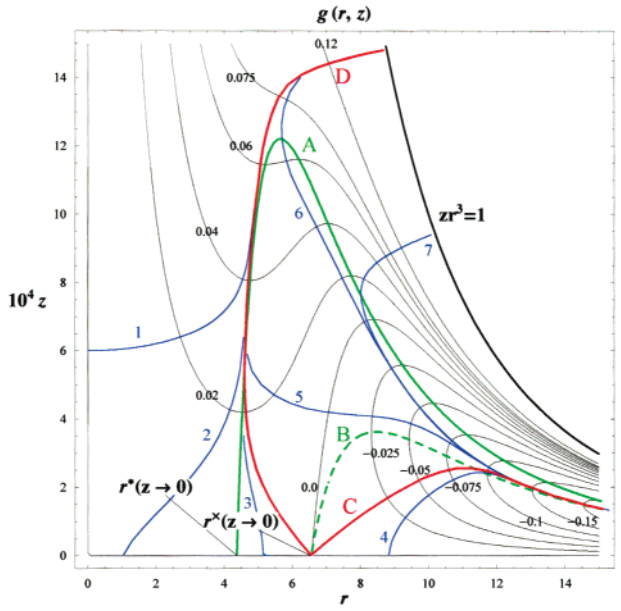

Figure 2. Contour plot of the Gibbs free energy of nucleation of silica particles, $g(r,z)$, small numbers near the contour lines, as a function of cluster size, r, and cluster concentration, z ($T = 310.15$ K, $y = 3$). For detailed explanation see text.

state is a consequence of the depletion of the mother phase during the particle formation. Graph A ends at the stable equilibrium of the bulk solid phase, plane surface, under saturation conditions. The amount contained in the solid is in this case $zr^3 = 1 - (1/y) = n_C^s(1)/n_L^0(1)$, and eq 2 reads $n_L^0(1) = n_L^s(1) + n_C^s(1)$. To guarantee that the radius is infinite at the plane surface, the logarithmic term in eq 12a must be exactly zero. This is obviously the case:

$$\lim_{zr^3 \to \frac{n_C^s(1)}{n_L^0(1)}} \left\{ \ln \frac{yb(1 - zr^3)}{1 - azr^3} \right\} = \ln \left\{ \frac{\frac{n_L^0(1)}{n_L^s(1)} \left(1 - \frac{n_C^s(1)}{n^0}\right)\left(1 - \frac{n_C^s(1)}{n_L^0(1)}\right)}{1 - \frac{n_C^s(1)}{n^0}} \right\} = 0 \quad (13)$$

Equation 12b determines the broken green graph labeled B. It is obtained by derivation of eq 11 with respect to z at constant r. The mathematical structure of eq 12b is similar to that of eq 12a. The difference is the factor 3/2 in the non-logarithmic term. Graph B starts at the radius $r^{\times}(z \to 0) = h/\ln(by) = 6.56$. This is the point where the potential function becomes again zero $g(r,z) = 0$. No difference exists to the reference state, the supersaturated solution without particles. Two extrema can be observed again up to the maximum of graph B. These two extrema are minima at the constant concentration of particles. The end point of graph B is also the stable equilibrium of bulk solid under saturation concentration.

Further graphs, the red lines labeled C and D and seven blue lines labeled by the corresponding numbers, follow the strongest change of the potential function, steepest decent or increase, i.e., the gradient of $g(r,z)$. The gradient is given by

$$\nabla g(r,z) = \left(\frac{\partial g(r,z)}{\partial r}\right)_z e_r + \left(\frac{\partial g(r,z)}{\partial z}\right)_r e_z \quad (14)$$

where e_r and e_z are the unit vectors in the r- and z-directions, respectively. It can be shown by simple geometrical considerations that the gradient curves in the contour plot are given by the following differential equation[8]

$$\frac{dz}{dr} = \frac{\left(\frac{\partial g(r,z)}{\partial z}\right)_r}{\left(\frac{\partial g(r,z)}{\partial r}\right)_z}. \quad (15)$$

Equation 15 cannot be solved analytically. The gradient curves have to be determined by numerical integration or by an appropriate mathematical procedure, which calculates the gradient curve from point to point at the surface. Both these methods are applied in the present considerations.

A thermodynamic system develops in the direction of the strongest change of the potential function, i.e., in the direction of the gradient curves to become more stable; that is, a more negative value of the potential function. The larger the particles, the smaller the gradient. Therefore, some problems arise for the numerical calculations according to the step size. So far, the two red and seven blue graphs are examples for the development of the system. Now an arbitrary point on graph 1 may be selected. This means the chosen system consists of particles of size and concentration given by the r and z coordinates of this point. The remaining amount of the particle-forming species is dissolved. The system develops in the direction of steepest decrease of $g(r,z)$ following line 1. The smallest value of $g(r,z)$ is attained at the z-axis, $r = 0$. These particles tend to dissolve. If a point on graph 2 gives the arbitrary composition of the system, the system develops until z becomes zero. Again the particles dissolve. A start configuration of the system that has coordinates given by a point on graphs 4 to 7 can follow the direction of more and more negative $g(r,z)$. All these curves approach quickly the red line labeled C. Consequently, the graph C fixes the bottom of the valley of the Gibbs free energy of particle formation. The valley ends at the stable equilibrium of the bulk solid phase in contact with the saturated solution. The corresponding value of $g(r,z)$ is the Gibbs free energy of the bulk liquid ($r = \infty$), g^b. It is

$$\lim_{zr^3 \to (1 - 1/y)} g(r,z) = g^b = -\ln y - \frac{1}{a}\left\{1 - a\left(1 - \frac{1}{y}\right)\right\} \ln\left\{1 - a\left(1 - \frac{1}{y}\right)\right\} - \left(1 - \frac{1}{y}\right)\ln b = -\ln y - \frac{1}{a}\ln b \quad (16)$$

A special feature can be observed in the case of graph 3. As can be seen, the system would begin at a chosen start position, developing in the vicinity of the r-axis, and then move nearly parallel to the r-axis in the direction of $r^{\times}(z \to 0)$. Furthermore, the system can follow graph C. All chosen compositions of the system between graphs A and D show this behavior up to the intersection point of both graphs. The first part of graph A up to the intersection point with graph D is therefore a borderline. This border between dissolution of particles and growth starts at $r^*(z \to 0)$, follows graph A, and after the intersection point of graphs A and D it follows graph D. Particles in states with compositions on the left-hand side of this line tend to dissolve. Particles in states on the right-hand side of this line tend to approach quickly the bottom of the valley of $g(r,z)$ to follow this line further.

Now the development of the system beginning at the reference state of the completely dissolved particle-forming species shall be followed. First, the system must overcome the maximum of $g(r,z)$ given by $r^*(z\rightarrow 0)$. Then the particles can grow to a size given by $r^{\times}(z\rightarrow 0)$. This process is analogous to the classical nucleation theory. Then, the system can follow the bottom of the $g(r,z)$ surface, i.e. graph C, beginning at $r^{\times}(z\rightarrow 0)$, up to the maximum of graph C; both the size and the concentration of the particle increase. This behavior may be called a nucleation phase. After passing the maximum of graph C, the particles grow further on but their concentration reduces. This behavior is usually called Ostwald ripening.

3. The Kinetic Model

As discussed in the previous paragraph, an arbitrary state of a system on the $g(r,z)$ surface consists of nanoparticles of uniform size having a determined concentration, and the remaining part of the total amount of particle forming substance is solute. The Gibbs free energy of this state is always larger than that of the stable equilibrium of the bulk solid under saturation concentration, $g(r,z) > g^b$. Therefore, any state of the system on the right-hand side of the borderline A−D tends to pass into this only stable state. Any such trajectory approaches quickly the bottom of the $g(r,z)$ surface. This bottom is the last part of the path of the system in its equilibrium. The trajectory of the system is assumed to follow the negative direction of the gradient of $g(r,z)$. If these gradient curves are calculated, the composition of the system on its path into the stable equilibrium is known. But nothing is known about the time dependence of this process. In accordance with common irreversible thermodynamics, the following ansatz is applied[9]

$$\frac{\mathrm{d}c_{\mathrm{L}}^{1}(1)}{\mathrm{d}t} = -\,kB\{c_{\mathrm{L}}^{1}(1)\}\,|\nabla g(r,z)| \qquad (17)$$

The concentration of the particle-forming species in the solution $c_{\mathrm{L}}{}^{1}(1)$ as function of time, t, is assumed to be proportional to the magnitude of the gradient of $g(r,z)$. The term k is the rate constant, and $B\{c_{\mathrm{L}}{}^{1}(1)\}$ is a coefficient, which may depend on the concentration. The temperature is constant and uniform throughout the whole system in the process considered. Equation 17 can be separated into a concentration-dependent part and a time-dependent part. Both parts must be equal to the same constant, m. The concentration dependent part, $\mathrm{d}c_{\mathrm{L}}{}^{1}(1)/B\{c_{\mathrm{L}}{}^{1}(1)\}$, can be obtained by the numerical integration. The concentration depends on the size and number of particles in the system. The relation between the number and the radius of the particles can be obtained by integration of eq 15. By this way the concentration can be calculated in dependence on the number of particles, z, or the radius of the particles, respectively. The time dependent part is $-k|\nabla g(r,z)|\mathrm{d}t$. It is assumed that the time is inversely proportional to the amount of the gradient of $g(r,z)$. It can also be integrated numerical in dependence on the number of particles or the radius of the particles, respectively, since the gradient may be calculated for each point on the surface of the potential function. This procedure is also possible only by numerical methods. To do the necessary calculations, the software Mathematica is used.[10] First, by integration of eq 15 the trajectory of the system has to be determined from a given start point. The integration must be done in such way that the resulting function $z(r)$ or $r(z)$ is unique. From the resulting curves, all necessary quantities such as concentration, magnitude of the gradient, or specific surface area can be calculated. Second, the time is determined by $t = -\mathrm{m}\int \mathrm{d}\xi/\,k|\nabla g(r,z)|$ as function of concentration. ξ stands for r or z, respectively. The numerical integration is not able to find the exact zero point because of a finite step width. By addition of a small constant, the time scales of the calculations and the experiments can be adapted. The rate constant can be determined by fitting the theoretical curve to the experimental points, as is common in kinetic evaluations. This procedure is valid as well for the formation of colloidal particles as for their dissolution.

4. Experiments

The model considerations shall now be used to make a comparison to experimental results. Dissolution experiments are available and are suitable. The dissolution of silica nanoparticles (HDK 30, Wacker Chemie GmbH) has been measured. 600 mg of this substance are dissolved in 0.5 L of water. The dissolution experiments are carried out at a temperature of 310 K, and the pH value has been adjusted to be pH = 7.33 by a buffer solution. One liter of this solution contains 35.4 mL 1N HCl, 6.54 g NaCl, and 6.1 g Tris(hydroxymethyl)-amino-methane. The radius of the primary particles has been determined from the BET surface area to be 4.5 nm. This is in accordance with data of the firm. The amount dissolved has been determined by the method of Motomitzu et al.[11] in dependence on dissolution time. For some selected samples, the specific BET surface area has been measured by use of an Autosorb-1 (Quantachrome GmbH). Details about the experimental data can be found in ref 12.

5. Comparison of Experimental Results and Theory

It is worth mentioning that in the case of the silica dissolution, water is consumed. This would violate the condition of constant amount of species 2: in the case discussed here it is $n_{\mathrm{L}}{}^{0}(2) \gg n_{\mathrm{L}}{}^{0}(1)$. So it may be justified to do the calculations under the assumption of the constancy of species 2. From the data given in section 4, an initial supersaturation in the system of $y = 9.986$ can be calculated. The constants $a = 3.628\ 10^{-4}$ and $b = 0.99967$ have somewhat other numerical values than that given for $y = 3$. At the beginning of the dissolution process, the whole amount of silica is contained in the particles. This is the point of $r = 20.3$ and $z = 20.3$ on the graph $zr^3 = 1$ shown in the contour plot of the $g(r,z)$ surface that is calculated for the experimental conditions, see Figure 3. The axes are scaled in such way that the start point has the same r and z value and that the unit vectors in the both directions are equal. This point where the whole amount of silica is contained in the particles is always the start point of integration. The dashed curve is the trajectory of steepest descent. It approaches quickly the bottom of the $g(r,z)$ surface (curve labeled C). As can be seen in the first time of the dissolution, the particles become smaller and their concentration is reduced. Following the bottom, the size of the particles increases and the concentration is reduced, Ostwald ripening. For the interpretation of the experimental data the trajectory of the system must be calculated over a larger range of radii. This is done by the way described in section 3. The experimental results are shown in Table 1 and Figure 4. Squares represent experimental data points, and the model calculates the solid black line.

The numerical integration can begin at exactly $t = 0$ and $c_{\mathrm{L}}{}^{1}(1) = 0$ if this point is added to experimental results. In these calculations a somewhat different procedure is applied. The slope of the concentration−time curve is very steep at small dissolution times. The deviations of the first experimental points, therefore, mainly influence the correlation coefficient. The start points of the measurements and the model calculations therefore were adjusted via the addition of an appropriate small constant.

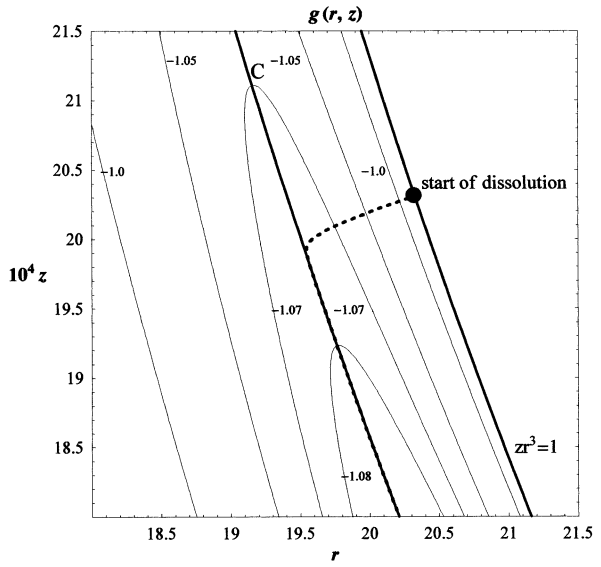

Figure 3. Contour plot of the Gibbs free energy of nucleation of silica particles, $g(r,z)$, small numbers near the contour lines, in the vicinity of the start point of dissolution as a function of cluster size, r, and cluster concentration, z ($T = 310.15$ K, $y = 9.986$).

TABLE 1: Concentration, $c_L^1(1)$ and BET Surface Area, O_{BET}, Measured as Function of Dissolution Time, t, for the Dissolution of Silica

t/h	$c_L^1(1)$/mmol L^{-1}	O_{BET}/m^{2}g^{-1}
0		305.3
0.4	0.68, 0.72, 0.74, 0.72	
5	2.51	
7.5	2.44	
16	2.59	
18	2.50, 2.50, 2.61, 2.60, 2.56, 2.62, 2.55, 2.50	311.9
23.6	2.52	
42	2.56, 2.54, 2.54, 2.56	310.8
49.6	2.4	
66	2.40, 2.43, 2.36, 2.38	
71.9	2.46	
180		240.2
186	2.48, 2.43, 2.51, 2.54	
197	2.54	
234	2.45, 2.41, 2.40, 2.37	
280		218
330	2.44, 2.31, 2.40, 2.39	205

The adjustment of the theoretical curve is done in that way such that there is no difference between the mean of the first four measured concentrations $c_L^1(1)\{t_1 = 0.4\ \text{h}\} = 0.715$ m mol L^{-1} and the calculated value. This adjustment is not necessary for drawing the concentration−time curve. Since the constant is very small. The procedure described assumes the mean of the first experimental points to be without error.

Somewhat more problematic is the fixation of the end point of the calculations. It could be used in some boundaries as free parameter. In the calculations it is chosen in such way that the measured concentrations at the longest dissolution time are in the vicinity of the calculated values, e.g., determination of the largest correlation coefficient. The rate constant is not a free parameter if it is accepted that the theoretical calculations should be carried out up to the longest experimental dissolution time. In this case the rate constant has a determined value. The only fitting parameter is therefore the last $r-z$ pair on the bottom of the $g(r,z)$ curve included in the calculation, the integration range. The limit of the integration determines the rate constant of dissolution. The influence of the last $r-z$ pair included in the calculations is shown in Figure 4. In case of the black curve, the integration is done in the range of $z = 20.3$ up to $z = 2.0$ and $r = 20.3$ up to $r = 42.2$. The particle size at the end of integration is 9.35 nm. The rate constant is found to be $k = 18.2$ h^{-1}. In case of the dashed curve the integration is done up to $z = 1$ and $r = 53.25$. The particle size at the end of integration is now 11.8 nm. The rate constant is determined to be 20 h^{-1}. Shortening of the integration range up to $z = 3$ and $r = 36.83$ leads to the dotted curve. The radius at the end of the integration range is now 8.16 nm and the rate constant is $k = 18.2$ h^{-1}. The influence of the integration range on the rate constant is small. The correlation coefficient of the black curve in Figure 4 compared to the experimental values is calculated to be 0.982648. In case of the dashed curve 0.984022 is obtained, and in case of the dotted curve 0.982462 is obtained. The goodness in all three cases is comparable.

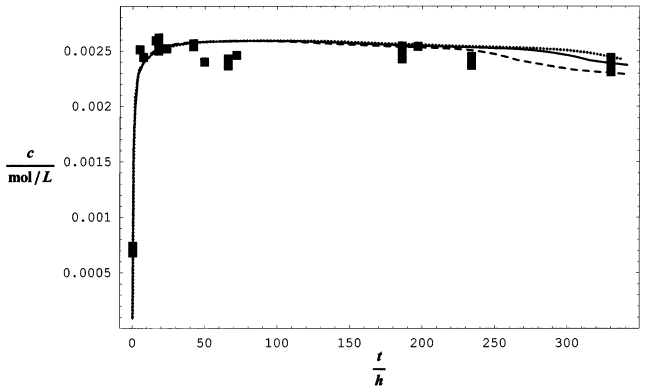

Figure 4. Concentration of the dissolved amount of silica $c_L^1(1)$ as function of time, t. Experimental results are represented by the squares. The theoretical calculations are carried out up to different final particle sizes: 8.16 nm (dotted line), 9.35 nm (black line), 11.8 nm (dashed line).

A detailed investigation shows that this rate constant can be expressed in terms of several elementary reactions that involve neutral, positively, and negatively charged species on the surface of the particles. By this way the kinetic constants of dissolution and precipitation can be expressed as function of pH and background electrolyte concentration.[13,14]

The specific surface area can also be calculated as function of dissolution time from the trajectory of the system since the $r-z$ pairs are fixed. The model calculations are compared to experimental measured data, Table 1. Squares in Figure 5 represent the experimental data and the theoretical calculated curves correspond to the mentioned integration ranges. A reasonably good agreement between experiment and theory, black curve, is obtained. It is noteworthy that no parameter has been changed. The deviations, especially for longer dissolution times, are considerable if the other range of integration ($z = 1$ and $r = 53.25$) is applied, dashed curve in Figure 5. The general trends of the time dependence of the change of the surface area are in accordance.

The principal accordance between experiment and theory can be obtained by optimization of the integration range or the rate constant, respectively, the only adjustable parameter. To get a better fit one can think of a change of the physical constants of the system. These constants could be the saturation concentration of the solution of the bulk solid or the interfacial tension. Iler, ref 7, gives a detailed description and discussion of experimental results of the determination of these quantities. The final result is that the saturation concentration of silica depends strongly on the special sample used. For bulk amorphous silica values

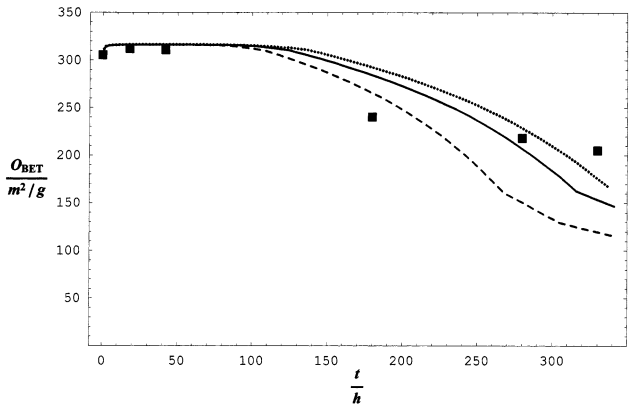

Figure 5. Specific surface area of the silica samples, O_{BET}, as function of dissolution time, *t*. Experimental results are represented by squares. The theoretical calculations are carried out up to different final particle sizes: 8.16 nm (dotted line), 9.35 nm (black line), 11.8 nm (dashed line).

between 1 mmol L^{-1} and 2 mmol L^{-1} are reported. Besides of the morphology of the samples, special constituents in the solution seem to be of influence. Our own experience with the dissolution of silica confirms the influence of the sample morphology. They show that the concentration of neutral silica monomer is relatively constant in a broad pH-region.[13] Increase of the monomer concentration in acidic and stronger in the basic regions results from charged monomeric species. In this consideration a saturation concentration of $c_L^s(1) = 2$ m mol/L for the bulk amorphous silica works well at 40 °C. This is in accordance with the data discussed by Iler, ref 7 pp 40. It is clear that the saturation concentration depends on the temperature. For a porous silica gel the solubility has been measured at 25, 45, and 55 °C, and saturation concentrations of 1.31, 2.80, and 3.11 m mol L^{-1} have been found.[15] To get the correct saturation concentration for the conditions under consideration requires several experiments with the same silica at different conditions. In view of our model calculations it could make sense to use the saturation concentrations as a second fitting parameter. On the other hand, the data of the interfacial tension given by Iler, ref 7 p 54, also show an influence of the preparation conditions and therefore of the sample morphology. The values are determined for 25 °C. The measurements are carried out at 37 °C. There may also be an influence of the temperature. The calculations have been carried out using a value of 50 mN m^{-1}. This seems to be reasonable since the values reported in ref 7 p 54 are 46 mN m^{-1} and 54 mN m^{-1}. On the other hand, the good agreement between experiment and theory found in our example shows that the data given by Iler seem to be correct. The scatter of the experimental results of dissolution, see Table 1, avoids questioning the accuracy of the physical constants.

6. Conclusions

A theoretical model has been presented for the formation and dissolution of colloid dispersed particles in aqueous solution. In the frame of this model the total amount of the particle-forming species is distributed on particles of uniform size, *r*. The particles have a determined concentration, *z*. The remaining part of the particle-forming species is dissolved in the solution as monomer. There are an infinite number of possibilities to build up such a system if the total amount of substance of the particle forming species is large. The only condition to be maintained is mass conservation. The Gibbs free energy of particle formation, $g(r,z)$, of each of these states is calculated compared to a reference system. The reference system is obtained if the complete amount of particle forming species is dissolved in the solution as monomer. This is the state of highest possible supersaturation in the system. The monomer is thought to consist of uncharged particles. It has been shown that this is the case in a relatively large range of pH for silica.[13] The influence of pH and charged species on dissolution and precipitation is also discussed in this contribution and ref 14. It has been shown that the rate constants of precipitation and dissolution, respectively, strongly depend on the pH of the solution and on the concentration of background electrolyte.

By partial derivation of $g(r,z)$ with respect to *r* and *z*, states of the system can be selected that have extremal properties. If the derivation is carried out at constant *z*, an equation is obtained which is similar to the familiar Kelvin equation. One new aspect is the variable supersaturation caused by the consumption of the mother phase by the particle formation. Mathematically the obtained equation contains an additional factor compared to the Kelvin equation. This factor guarantees thermodynamic consistency. In the present case where the solubility of the particles is very small, the factor is nearly one. For substances having higher solubility it would become remarkable. An equation for extrema of the same mathematical structure can be obtained by the derivation of $g(r,z)$ with respect to *z* at constant *r*. The difference is only a factor of 3/2 in the non-logarithmic term.

Curves of steepest descent or ascent of the potential function, $g(r,z)$, gradient curves, can also be calculated at the surface. If one selects an arbitrary point at the $g(r,z)$ surface, it is assumed that the system develops in the direction of negative gradient $g(r,z)$, i.e., in the direction of the gradient curves. By this means the states at the $g(r,z)$ surface may be divided into states where the particles tend to dissolve and states where the system quickly approaches the bottom of the valley of the $g(r,z)$ surface. The bottom ends at stable equilibrium of the bulk phase of the particle-forming species having a plane surface at saturation concentration. The bottom of the valley is determined neither by the Kelvin equation nor by the equation obtained by derivation with respect to *z*. The graph of the bottom can be obtained by integration of a differential equation that contains the quotient of both partial derivatives, eq 15. The integration must start at $r^{\times}(z \rightarrow 0)$ for determination of the bottom line.

The model offers a plausible method for the formation of nanoparticles from a supersaturated initial solution. After overcoming the critical state first it follows a nucleation phase where concentration and size of the particles increase. Later on in time the particles grow, but the concentration reduces. This is the phase of Ostwald ripening.

It seems worth mentioning that the formation of liquid droplets from a supersaturated mixture of a condensing substance with a carrier gas can be successfully described by analogous considerations.[6,16]

On the other hand, the trajectory of a given amount of nanoparticles during the dissolution process can be followed. This path starts at the point determined by the radius and the concentration of the particles. It approaches the bottom of the free energy surface and it ends at the stable equilibrium, bulk phase in the saturated solution. The slope of the bottom becomes smaller and smaller with increasing size of the particles. Physically, a small slope of the bottom means very small rate of changes of the system. Systems in these states are therefore relatively stable even without additional stabilization. This is

in accordance with the observation that precipitates of nanoparticle size coming in the vicinity of the μm range are relative stable.

Experiments have been carried out to determine the dissolution of silica nanoparticles. The general course of the experimental curve can be described well by the model presented. It is interesting that the experimentally determined change of the specific surface area of the particles during the dissolution is also described well without additional assumptions or corrections. In this context it must be mentioned that the electrolyte solution must be removed from the samples prior to the determination of the specific surface area. Washing with pure water does this. Since the dissolution starts very rapidly in the first period of time, a change of the surface area by the washing is possible. The nice accordance between experimental values and theoretical calculations, therefore, has to be confirmed by further measurements. Nevertheless, it is convincing that the experimental dissolution curve and the development of the surface area of the sample in time can be described without any change of the parameter. The only parameter of the model calculations is the rate constant of dissolution which is fixed by the range of integration. It is determined by the experiments. This is the common situation in the evaluation of kinetic experiments.

References and Notes

(1) Ellerby, H. M.; Weakliem, C. L.; Reiss, H. *J. Chem. Phys.* **1991**, *95*(12), 9209.

(2) Senger, B.; Schaaf, P.; Corti, D. S.; Bowles, R. K.; Voegel, J.-C.; Reiss, H. *J. Chem. Phys*. **1999**, *110*(13), 6421.

(3) Reguera, D.; Bowles, R. K.; Djikaev, Y.; Reiss, H. *J. Chem. Phys.* **2003**, *118*(1), 340.

(4) Münster, A. *Chemische Thermodynamik*; Akademie-Verlag: Berlin, 1969; p 84.

(5) Atkins, P. W. *Physical Chemistry*; Oxford University Press: Oxford, Melbourne, Tokyo, 1992; p 182.

(6) Vogelsberger, W. *J. Phys. Chem. B* **2001**, *105*(47), 11559.

(7) Iler, R. K. *The Chemistry of Silica*; J. Wiley & Sons: New York, 1979; p 54.

(8) Vogelsberger, W.; Beck, M.; Fritsche, M.; Mäurer, F. *Z. Phys. Chem*. **1992**, *175*, 201.

(9) Kluge, G.; Neugebauer, G. *Grundlagen der Thermodynamik*; VEB Deutscher Verlag der Wissenschaften: Berlin, 1976; p 241.

(10) Wolfram, S. *Mathematica* 3. Auflage, Bonn, et al., Addison-Wesley: Reading, MA, 1997.

(11) Motomizu, S.; Oshima, M.; Ojima, Y. *Anal. Sci*. **1989**, *5*, 85.

(12) Thron, D., *diploma theses*, F.-Schiller-University, Jena, 2001.

(13) Löbbus, M.; Vogelsberger, W.; Sonnefeld, J.; Seidel, A. *Langmuir* **1998**, *14*(16), 4386.

(14) Vogelsberger, W.; Seidel, A.; Breyer,T. *Langmuir* **2002**, *18*(8), 3027.

(15) Vogelsberger, W.; Mittelbach, T.; Seidel, A. *Ber. Bunsen-Ges. Phys. Chem*. **1996**, *100*(7) 1118.

(16) Rodemann, T.; Peters, F. *J. Chem. Phys*. **1996**, *105*(12), 5168.